Measurement of the $b \to \tau^- \overline{\nu}\_\tau X$ branching ratio

D. Buskulic, D. Decamp, C. Goy, J P. Lees, M N. Minard, B. Mours, R. Alemany, F. Ariztizabal, P. Comas, J M. Crespo, et al.

EUROPEAN ORGANIZATION FOR NUCLEAR RESEARCH

Measurement of the $b \rightarrow \tau^- \bar{\nu}_\tau X$ Branching Ratio

The ALEPH Collaboration[*]

Abstract

Using a missing energy tag, evidence is presented for the decay $b \rightarrow \tau^- \bar{\nu}_\tau X$, and its branching ratio is measured to be $4.08 \pm 0.76 \pm 0.62\%$.

(Submitted to Physics Letters B.)

[*] See following pages for the author list.

The ALEPH Collaboration

D. Buskulic, D. Decamp, C. Goy, J.-P. Lees, M.-N. Minard, B. Mours

Laboratoire de Physique des Particules (LAPP), IN²P³-CNRS, 74019 Annecy-le-Vieux Cedex, France

R. Alemany, F. Ariztizabal, P. Comas, J.M. Crespo, M. Delfino, E. Fernandez, V. Gaitan, Ll. Garrido, T. Mattison, A. Pacheco, A. Pascual

Institut de Fisica d'Altes Energies, Universitat Autonoma de Barcelona, 08193 Bellaterra (Barcelona), Spain[7]

D. Creanza, M. de Palma, A. Farilla, G. Iaselli, G. Maggi, M. Maggi, S. Natali, S. Nuzzo, M. Quattromini, A. Ranieri, G. Raso, F. Romano, F. Ruggieri, G. Selvaggi, L. Silvestris, P. Tempesta, G. Zito

INFN Sezione di Bari e Dipartimento di Fisica dell' Università, 70126 Bari, Italy

H. Hu,[20] D. Huang, X. Huang, J. Lin, J. Lou, C. Qiao,[20] T. Wang, Y. Xie, D. Xu, R. Xu, J. Zhang, W. Zhao

Institute of High-Energy Physics, Academia Sinica, Beijing, The People's Republic of China[8]

L.A.T. Bauerdick,[24] E. Blucher, G. Bonvicini, F. Bossi, J. Boudreau, D. Casper, H. Drevermann, R.W. Forty, G. Ganis, C. Gay, R. Hagelberg, J. Harvey, S. Haywood, J. Hilgart, R. Jacobsen, B. Jost, J. Knobloch, E. Lançon, I. Lehraus, T. Lohse,[32] A. Lusiani, M. Martinez, P. Mato, H. Meinhard, A. Minten, R. Miquel, H.-G. Moser, P. Palazzi, J.A. Perlas, J.-F. Pusztaszeri,[30] F. Ranjard, G. Redlinger,[25] L. Rolandi, J. Rothberg,[2] T. Ruan,[20,27] M. Saich, D. Schlatter, M. Schmelling, F. Sefkow, W. Tejessy, H. Wachsmuth, W. Wiedenmann, T. Wildish, W. Witzeling, J. Wotschack

European Laboratory for Particle Physics (CERN), 1211 Geneva 23, Switzerland

Z. Ajaltouni, F. Badaud, M. Bardadin-Otwinowska, A.M. Bencheikh, R. El Fellous, A. Falvard, P. Gay, C. Guicheney, P. Henrard, J. Jousset, B. Michel, J-C. Montret, D. Pallin, P. Perret, B. Pietrzyk, J. Proriol, F. Prulhière, G. Stimpfl

Laboratoire de Physique Corpusculaire, Université Blaise Pascal, IN²P³-CNRS, Clermont-Ferrand, 63177 Aubière, France

T. Fearnley, J.D. Hansen, J.R. Hansen,[1] P.H. Hansen, R. Møllerud, B.S. Nilsson

Niels Bohr Institute, 2100 Copenhagen, Denmark[9]

I. Efthymiopoulos, A. Kyriakis, E. Simopoulou, A. Vayaki, K. Zachariadou

Nuclear Research Center Demokritos (NRCD), Athens, Greece

J. Badier, A. Blondel, G. Bonneaud, J.C. Brient, G. Fouque, S. Orteu, A. Rosowsky, A. Rougé, M. Rumpf, R. Tanaka, M. Verderi, H. Videau

Laboratoire de Physique Nucléaire et des Hautes Energies, Ecole Polytechnique, IN²P³-CNRS, 91128 Palaiseau Cedex, France

D.J. Candlin, M.I. Parsons, E. Veitch

Department of Physics, University of Edinburgh, Edinburgh EH9 3JZ, United Kingdom[10]

L. Moneta, G. Parrini

Dipartimento di Fisica, Università di Firenze, INFN Sezione di Firenze, 50125 Firenze, Italy

M. Corden, C. Georgiopoulos, M. Ikeda, J. Lannutti, D. Levinthal,[15] M. Mermikides[†], L. Sawyer, S. Wasserbaech

Supercomputer Computations Research Institute and Dept. of Physics, Florida State University, Tallahassee, FL 32306, USA [12,13,14]

A. Antonelli, R. Baldini, G. Bencivenni, G. Bologna,[4] P. Campana, G. Capon, F. Cerutti, V. Chiarella, B. D'Ettorre-Piazzoli,[26] G. Felici, P. Laurelli, G. Mannocchi,[5] F. Murtas, G.P. Murtas, L. Passalacqua, M. Pepe-Altarelli, P. Picchi[4]

Laboratori Nazionali dell'INFN (LNF-INFN), 00044 Frascati, Italy

B. Altoon, O. Boyle, P. Colrain, I. ten Have, J.G. Lynch, W. Maitland, W.T. Morton, C. Raine, J.M. Scarr, K. Smith, A.S. Thompson, R.M. Turnbull

Department of Physics and Astronomy, University of Glasgow, Glasgow G12 8QQ,United Kingdom[10]

B. Brandl, O. Braun, C. Geweniger, P. Hanke, V. Hepp, E.E. Kluge, Y. Maumary, A. Putzer, B. Rensch, A. Stahl, K. Tittel, M. Wunsch

Institut für Hochenergiephysik, Universität Heidelberg, 6900 Heidelberg, Fed. Rep. of Germany[16]

A.T. Belk, R. Beuselinck, D.M. Binnie, W. Cameron, M. Cattaneo, D.J. Colling, P.J. Dornan, S. Dugeay, A.M. Greene, J.F. Hassard, N.M. Lieske, J. Nash, S.J. Patton, D.G. Payne, M.J. Phillips, J.K. Sedgbeer, I.R. Tomalin, A.G. Wright

Department of Physics, Imperial College, London SW7 2BZ, United Kingdom[10]

E. Kneringer, D. Kuhn, G. Rudolph

Institut für Experimentalphysik, Universität Innsbruck, 6020 Innsbruck, Austria[18]

C.K. Bowdery, T.J. Brodbeck, A.J. Finch, F. Foster, G. Hughes, D. Jackson, N.R. Keemer, M. Nuttall, A. Patel, T. Sloan, S.W. Snow, E.P. Whelan

Department of Physics, University of Lancaster, Lancaster LA1 4YB, United Kingdom[10]

K. Kleinknecht, J. Raab, B. Renk, H.-G. Sander, H. Schmidt, F. Steeg, S.M. Walther, B. Wolf

Institut für Physik, Universität Mainz, 6500 Mainz, Fed. Rep. of Germany[16]

J-J. Aubert, C. Benchouk, A. Bonissent, J. Carr, P. Coyle, J. Drinkard, F. Etienne, S. Papalexiou, P. Payre, Z. Qian, L. Roos, D. Rousseau, P. Schwemling, M. Talby

Centre de Physique des Particules, Faculté des Sciences de Luminy, IN^2P^3-CNRS, 13288 Marseille, France

S. Adlung, C. Bauer, W. Blum,[1] D. Brown, P. Cattaneo,[31] G. Cowan, B. Dehning, H. Dietl, F. Dydak,[23] M. Fernandez-Bosman, M. Frank, A.W. Halley, J. Lauber, G. Lütjens, G. Lutz, W. Männer, R. Richter, H. Rotscheidt, J. Schröder, A.S. Schwarz, R. Settles, H. Seywerd, U. Stierlin, U. Stiegler, R. St. Denis, M. Takashima,[3] J. Thomas,[3] G. Wolf

Max-Planck-Institut für Physik, Werner-Heisenberg-Institut, 8000 München, Fed. Rep. of Germany[16]

J. Boucrot, O. Callot, A. Cordier, M. Davier, J.-F. Grivaz, Ph. Heusse, D.E. Jaffe, P. Janot, D.W. Kim,[19] F. Le Diberder, J. Lefrançois, A.-M. Lutz, M.-H. Schune, J.-J. Veillet, I. Videau, Z. Zhang,

Laboratoire de l'Accélérateur Linéaire, Université de Paris-Sud, IN^2P^3-CNRS, 91405 Orsay Cedex, France

D. Abbaneo, S.R. Amendolia, G. Bagliesi, G. Batignani, L. Bosisio, U. Bottigli, C. Bozzi, C. Bradaschia, M. Carpinelli, M.A. Ciocci, R. Dell'Orso, I. Ferrante, F. Fidecaro, L. Foà, E. Focardi, F. Forti, A. Giassi, M.A. Giorgi, F. Ligabue, E.B. Mannelli, P.S. Marrocchesi, A. Messineo, F. Palla, G. Rizzo, G. Sanguinetti, P. Spagnolo, J. Steinberger, R. Tenchini, G. Tonelli, G. Triggiani, C. Vannini, A. Venturi, P.G. Verdini, J. Walsh

Dipartimento di Fisica dell'Università, INFN Sezione di Pisa, e Scuola Normale Superiore, 56010 Pisa, Italy

J.M. Carter, M.G. Green, P.V. March, Ll.M. Mir, T. Medcalf, I.S. Quazi, J.A. Strong, L.R. West

Department of Physics, Royal Holloway & Bedford New College, University of London, Surrey TW20 OEX, United Kingdom[10]

D.R. Botterill, R.W. Clifft, T.R. Edgecock, M. Edwards, S.M. Fisher, T.J. Jones, P.R. Norton, D.P. Salmon, J.C. Thompson

Particle Physics Dept., Rutherford Appleton Laboratory, Chilton, Didcot, Oxon OX11 OQX, United Kingdom[10]

B. Bloch-Devaux, P. Colas, H. Duarte, W. Kozanecki, M.C. Lemaire, E. Locci, S. Loucatos, E. Monnier, P. Perez, F. Perrier, J. Rander, J.-F. Renardy, A. Roussarie, J.-P. Schuller, J. Schwindling, D. Si Mohand, B. Vallage

Service de Physique des Particules, DAPNIA, CE-Saclay, 91191 Gif-sur-Yvette Cedex, France[17]

R.P. Johnson, A.M. Litke, G. Taylor, J. Wear

Institute for Particle Physics, University of California at Santa Cruz, Santa Cruz, CA 95064, USA[29]

J.G. Ashman, W. Babbage, C.N. Booth, C. Buttar, R.E. Carney, S. Cartwright, F. Combley, F. Hatfield, P. Reeves, L.F. Thompson[1]

Department of Physics, University of Sheffield, Sheffield S3 7RH, United Kingdom[10]

E. Barberio, A. Böhrer, S. Brandt, C. Grupen, F. Rivera, U. Schäfer

Fachbereich Physik, Universität Siegen, 5900 Siegen, Fed. Rep. of Germany[16]

G. Giannini, B. Gobbo, F. Ragusa[22]

Dipartimento di Fisica, Università di Trieste e INFN Sezione di Trieste, 34127 Trieste, Italy

L. Bellantoni, W. Chen, D. Cinabro,[28] J.S. Conway, D.F. Cowen,[21] Z. Feng, D.P.S. Ferguson, Y.S. Gao, J. Grahl, J.L. Harton, R.C. Jared,[6] B.W. LeClaire, C. Lishka, Y.B. Pan, J.R. Pater, Y. Saadi, V. Sharma, M. Schmitt, Z.H. Shi, A.M. Walsh, F.V. Weber, M.H. Whitney, Sau Lan Wu, X. Wu, G. Zobernig

Department of Physics, University of Wisconsin, Madison, WI 53706, USA[11]

1 Introduction

The Standard Model prediction for the $b \to \tau^- \bar{\nu}_\tau X$ branching ratio is $2.83 \pm 0.31\%$ [1], where the error is due to uncertainty in the form factors of the decay. It is thus one of the larger, as yet undetected decay modes of the b hadron. Furthermore, under certain conditions, two Higgs doublet models can predict $b \to \tau^- \bar{\nu}_\tau X$ branching ratios of 10-20% [2].

The presence of the two ν_τ in the decay chain $b \to \tau^- \bar{\nu}_\tau X$, $\tau^- \to \nu_\tau X'$ makes it difficult to reconstruct. The analysis presented here therefore identifies the decay using the large missing energy associated with the two ν_τ.

2 The ALEPH Detector

A detailed description of the ALEPH detector can be found in [3]. A time-projection chamber (TPC) lying between radii of 31 and 180 cm measures up to 21 three-dimensional points for each track. It also provides dE/dx information, with a resolution of up to 4.4%, for particle identification. Inside the TPC is a drift chamber (ITC) which provides up to eight more hits per track, and inside this a two layer silicon vertex detector (VDET) with a resolution of 12 μm in both $r\phi$ and z. Together, these detectors give a momentum resolution of $\sigma_p/p^2 = 6.6 \times 10^{-4}$ (GeV/c)$^{-1}$. Outside the TPC is an e/γ calorimeter (ECAL), and beyond this, a superconducting solenoid providing a 1.5 T magnetic field. A 120 cm thick, 23 layer hadron calorimeter (HCAL) surrounds the solenoid, followed by two double layers of muon (streamer) chambers.

3 Analysis Method

Hadronic events were selected using charged tracks as in [4]. To eliminate residual $Z^0 \to \tau^+\tau^-$, two-photon and beam-gas events (present at the 0.2% level) which would otherwise have significantly biased the analysis, events were required to have at least seven charged tracks coming from the primary vertex and a missing energy of less than 50 GeV. These two cuts reject only 0.3% of hadronic events. A total of 169000 events were selected from the 1991 data, all with $\sqrt{s} = 91.2$ GeV. The analysis also used 380000 Monte Carlo events, which were generated using JETSET 7.2 (parton shower) [5], with b and c quark fragmentation according to the parameterization of Peterson *et al.* [6], and processed through a full simulation of the ALEPH detector.

The analysis proceeded as follows:

1) Events were required to have $|\cos\theta| < 0.7$, where θ is the angle between the thrust axis and the beam axis, and also to have a thrust of at least 0.85. The 55% of events passing these cuts were well contained in the detector.

2) Each event was divided into two hemispheres separated by the plane perpendicular to the thrust axis.

The visible energy, E_{vis}, in each hemisphere was obtained as in [7], by adding the total energy of the charged tracks, $E_{charged}$, of photons identified in the ECAL, E_{photon}, and of neutral hadrons, E_{neut}. The latter is the sum of all energy clusters in the calorimeters, after subtracting contributions from identified photons and muons, and contributions consistent with coming from charged tracks.

The missing energy, E_{miss}, in each hemisphere was then approximated by $E_{miss} = E_{beam} - E_{vis}$, where E_{beam} is one half of the centre-of-mass energy. This assumes that the true (visible plus invisible) energy in each hemisphere is E_{beam}: an assumption which, according to the Monte Carlo, is accurate to within 5 GeV for 99% of events having thrust greater than 0.85.

3) To reject background associated with ν_e and ν_μ (in particular from $b, \bar{c} \rightarrow e^-/\mu^- X$ decays), hemispheres were used only if no $e^\pm$ or $\mu^\pm$ were identified amongst the tracks passing within 2.5 cm of the primary vertex in the $r\phi$ projection and 7 cm of it in z. This cut rejected 53.2% of hemispheres in the data and 53.5% in the Monte Carlo.

To achieve a high veto efficiency for this background, the cuts used for the lepton identification were extremely loose:

i) Muon identification was attempted down to momenta of 1 GeV. Particles were assumed to be $\mu^\pm$ if they satisfied either:

$N_{fire} \geq 0.4 N_{exp}$ and $N_{10} \geq 3$,

or: $N_\mu \geq 2$ and $X_{mult} \leq 2$,

where N_{fire} is the number of planes in the HCAL which fired within a road around the track and N_{exp} is the number which a $\mu^\pm$ of that momentum would be expected to cross; N_{10} and N_3 are the number of planes which fired within the road in the last ten and the last three layers of the HCAL respectively; N_μ is the number of fired planes in the muon chambers and X_{mult} is the average hit multiplicity per layer in the HCAL, again both within the road around the track [8].

For particles with momenta of greater than 7 GeV, the requirement $N_{10} \geq 3$ was replaced by the requirement that $N_{10} \geq 5$, and either $N_3 \geq 1$ or $N_\mu \geq 1$.

ii) Particles were assumed to be $e^\pm$ if their dE/dx satisfied $\chi_e^2 < 9$ and $\chi_e^2 - \chi_\pi^2 < -7$, where χ_e (χ_π) is the difference between the measured dE/dx and that expected for an $e^\pm$ ($\pi^\pm$), divided by the estimated error on this difference. No explicit momentum cut was employed.

Particles with momenta in excess of 1 GeV and $\chi_e^2 < 9$ were also identified as $e^\pm$ if their longitudinal and transverse estimators in the ECAL, R_L and R_T, satisfied $|R_L| < 3$ and $R_T > -3$. The estimator R_T is based on a comparison of the measured track momentum with the energy deposited in the four ECAL towers closest to the extrapolated track, while R_L compares the measured longitudinal shower profile with that expected for an electron. For true $e^\pm$, both R_L and R_T have a roughly Gaussian distribution of unit width, centred at zero [8].

Hemispheres in which the only identified leptons are $e^\pm$ from gamma

conversions need not be eliminated. Conversions were recognized by searching for pairs of oppositely charged tracks, both identified as $e^{\pm}$, and neither passing within 0.2 cm of the primary vertex in the $r\phi$ projection. At their point of closest approach in this projection, the two tracks were additionally required to have a separation of less than 2 cm and an invariant mass of less than 20 MeV. Furthermore, this point was required to lie near one of the detector walls. This procedure flagged 28% of the $e^{\pm}$ from conversions, whilst incorrectly flagging only 1% of the $e^{\pm}$ from other sources.

4) Hemispheres in which the measured missing energy is large as a result of the finite detector resolution are another major source of background. As this problem is equally as likely to occur in light quark and $c\bar{c}$ events, as in $b\bar{b}$ events, this background can be reduced by a factor of roughly five by selecting $b\bar{b}$ events. This selection makes use of the relatively long b lifetime and the precision of the VDET. It proceeds as follows:

The tracks in each event are clustered into jets using the JADE algorithm [9]. The distance, D, of closest approach of each track to the primary vertex (in three dimensions) is calculated. D is given a positive sign if the vector joining the primary vertex to the point at which the track passes closest to the axis of its corresponding jet, makes an angle of less than 90° to the jet direction, or a negative sign otherwise. Detector resolution smears the D of tracks from the primary vertex according to a roughly Gaussian probability distribution $\rho(D)$, centred at $D = 0$. As tracks from the decay of long-lived particles such as b-hadrons nearly always have positive D, the region $D < 0$ is dominated by tracks from the primary vertex and hence can be used to measure the distribution $\rho(D)$. Knowing $\rho(D)$, a confidence level $\alpha_i = \int_{D_i}^{\infty} \rho(x)dx$ is calculated for each track, i, in an event, that it comes from the primary vertex. The confidence level α^{event} of an event containing N tracks is then defined as the probability that N tracks coming from the primary vertex could yield a value of $\prod_{i=1}^{N} \alpha_i$ less than the measured one. The confidence level of an event-hemisphere α^{hemi} is similarly defined.

The $b\bar{b}$ events are tagged by requiring $\alpha^{event} < 0.005$. The Monte Carlo indicates that this yields $b\bar{b}$ events with an efficiency of 77% and a purity of 81%. The performance on the data is somewhat worse and is discussed in Section 4.3.

4 Corrections to the Monte Carlo

The measurement of the $b \to \tau^- \bar{\nu}_\tau X$ branching ratio relies on a comparison of the E_{miss} spectrum in the data with that in the Monte Carlo. The missing energy resolution, $e^{\pm}/\mu^{\pm}$ identification efficiency and performance of the $b\bar{b}$ tag can however be measured using the data itself and then used to correct the simulation. This procedure is described in this Section. The associated systematics are discussed in Section 5.1.

4.1 The Missing Energy Resolution

To study the resolution, it is desirable to minimise the effect of semileptonic decays which otherwise distort the positive tail of the E_{miss} spectrum. This was achieved

by studying event-hemispheres selected virtually as in Section 3, but tagging light quark rather than $b\bar{b}$ events. This tag required $\alpha^{event} > 0.5$ and yielded light quark/$c\bar{c}$/$b\bar{b}$ events in the ratio 89:10:1 respectively.

The resultant data and Monte Carlo E_{miss} spectra are compared in Fig. 1a. They are in rather poor agreement. The purpose of this subsection will be to seek corrections to map the Monte Carlo spectrum onto the data one.

As a first step, the hemispheres were binned in a three-dimensional grid according to the fractional contributions to E_{vis} of the charged, photon and neutral hadronic energy components. The shape of the E_{miss} spectrum for the data in a given bin of this grid can only differ significantly from the corresponding Monte Carlo spectrum if the detector simulation is inaccurate. The largest discrepancies were found in hemispheres having a large proportion of neutral hadronic energy E_{neut}. This is thought to be caused by the Monte Carlo overestimating the number of nuclear interactions in the ALEPH magnet. Sensitivity to this poorly understood effect was reduced by only using hemispheres satisfying $E_{neut} < 7$ GeV in the analysis. 69.5% of hemispheres passed this cut in the data and 68.8% in the Monte Carlo.

Most of the discrepancy remaining after this cut was removed by scaling $E_{charged}$, E_{photon} and E_{neut} in the Monte Carlo hemispheres by factors of $f_{charged}$, f_{photon} and f_{neut} respectively. These parameters were obtained by minimising $\chi^2 = \sum_i (\Delta_i/\sigma_{\Delta i})^2$, where the sum extends over all the occupied bins in the grid, Δ_i is the difference between the mean values of E_{miss} in data and Monte Carlo in the ith bin, and $\sigma_{\Delta i}$ is the error on this difference. The results of this fit are given in Table 1. The large deviation of f_{neut} from unity confirms the problems with the neutral hadronic energy simulation.

After this recalibration, agreement between data and Monte Carlo was good, except in the region $E_{miss} > 10$ GeV, where the data was a factor of 1.2 higher than the Monte Carlo. For Monte Carlo hemispheres not containing semi-leptonic decays, this was corrected for simply by weighting the hemispheres in this region by the factor of 1.2. No corresponding correction was applied to hemispheres containing semi-leptonic decays: since the E_{miss} spectrum of these hemispheres is dominated by the semileptonic decay rather than detector resolution, problems in the tail of the resolution function have negligible effect on them.

The agreement between data and Monte Carlo after applying these corrections and the $E_{neut} < 7$ GeV cut is shown in Fig. 1b.

According to the Monte Carlo, the E_{miss} resolution is slightly better in $b\bar{b}$ than in light quark events, which suggests that the above corrections might not be appropriate for $b\bar{b}$ tagged events. Indeed, for hemispheres selected as above but using the $b\bar{b}$ rather than the light quark tag, the central peak of the E_{miss} spectrum is positioned at a value of E_{miss} which is 0.18 ± 0.04 GeV higher in the data than in the (recalibrated) Monte Carlo. Semileptonic b and c decays have a significant effect on the tails of these spectra, but not on the position of the central peak. This discrepancy therefore indicates that a further correction to the Monte Carlo resolution function is needed for $b\bar{b}$ tagged hemispheres. The E_{vis} of such

hemispheres was therefore scaled by an additional factor $f_{extra} = 0.996 \pm 0.001$.

When estimating the systematic errors on the $b \to \tau^- \bar{\nu}_\tau X$ branching ratio, allowance will be made for the possibility that the weights applied to the Monte Carlo in the region $E_{miss} > 10$ GeV are incorrect, and for the possibility that the factor f_{extra} is spurious (results from distortions caused by semileptonic decays).

4.2 The $e^\pm / \mu^\pm$ Identification Efficiency

The histograms in Figs. 2a,b show the efficiencies with which the $e^\pm / \mu^\pm$ from $b, \bar{c} \to e^- / \mu^- X$ decays are identified, as estimated using the Monte Carlo truth information.

For $e^\pm$ the efficiency was also estimated by selecting gamma conversions as in Section 3, but requiring only one track to be identified as an $e^\pm$, and then noting the probability of the other track being identified. Corrections were applied to compensate for the estimated 2.5% of these tracks which were not really $e^\pm$ and for the fact that $e^\pm$ in gamma conversions tend to have fewer dE/dx samples, as the two tracks are so close together. The resulting estimates of the $e^\pm$ identification efficiency in both data and Monte Carlo have been superimposed over Fig. 2a. For the Monte Carlo, this estimate is in good agreement with that given by the Monte Carlo truth for $b, \bar{c} \to e^- X$ decays. Small differences are visible between the data and the Monte Carlo however.

The identification efficiency for $\mu^\pm$ with momenta of over 3 GeV should be similar to that for $\mu^\pm$ in $Z^0 \to \mu^+ \mu^-$ events, as such $\mu^\pm$ are expected to pass through the entire HCAL. At lower momenta, the efficiency can be estimated from two-photon $\to \mu^+ \mu^-$ events. In both cases, events with the correct topology were selected in which one of the two particles was positively identified as a $\mu^\pm$. The $\mu^\pm$ identification efficiency was then obtained from the other track. It has been superimposed over Fig. 2b. Non-$\mu^\pm$ background was negligible amongst the $\mu^\pm$ candidates in $Z^0 \to \mu^+ \mu^-$ and below 1% in the two-photon $\to \mu^+ \mu^-$ events.

The $\mu^\pm$ identification efficiency estimated using Monte Carlo two-photon events is lower than that given by the Monte Carlo truth for $b, \bar{c} \to \mu^- X$ decays. This is because in hadronic events, a second particle will sometimes enter the same region of the HCAL as the $\mu^\pm$ and then fire layers of the HCAL which the $\mu^\pm$ failed to. Nonetheless a comparison of the $\mu^\pm$ identification efficiencies in data and Monte Carlo remains meaningful and reveals significant discrepancies in the momentum range 1-3 GeV. Below 1 GeV, the $\mu^\pm$ identification efficiency is zero. This fact causes about 50% of the $b, \bar{c} \to e^- / \mu^- X$ background in Fig. 3.

The effect of these discrepancies on the measured branching ratio is corrected for by weighting Monte Carlo hemispheres according to the number and momenta of any $e^\pm / \mu^\pm$ they contain from $b, \bar{c} \to e^- / \mu^- X$ decays. ($e^\pm / \mu^\pm$ from other sources will be discussed in Section 5.1.5).

4.3 The Performance of $b\bar{b}$ Tag

The performance of the $b\bar{b}$ tag on the data was estimated from the fraction of events passing a single hemisphere tag (requiring one hemisphere to satisfy $\alpha^{hemi} < $ cut)

and the fraction passing a double hemisphere tag (requiring both hemispheres to pass this cut). Assuming that for a given event flavour there is no correlation between the two hemispheres, these fractions are directly related to the hemisphere tagging efficiencies for $b\bar{b}$ and $c\bar{c}$ events. The single (double) hemisphere tagging efficiency for light quark events is equal to the cut value (cut value squared) as a result of the definition of α^{hemi}. The performance of the event tag can then be approximately related to that of the double hemisphere tag (to which it is slightly superior).

The tagging efficiencies of $b\bar{b}$ and $c\bar{c}$ events are found to be lower in the data than in the Monte Carlo by factors of 0.79 ± 0.10 and 0.82 ± 0.09 respectively. The errors on these numbers allow for the approximation just mentioned.

This discrepancy between data and Monte Carlo arises primarily because of an inaccurate simulation of multiple scattering in the VDET. It is corrected for by weighting the Monte Carlo $b\bar{b}$ and $c\bar{c}$ events by these factors.

5 Results

Fig. 3 shows the E_{miss} distribution for the (recalibrated) Monte Carlo and real data after applying all the cuts of Section 3. The histogram for the Monte Carlo has been subdivided into the contributions coming from: (i) $b \rightarrow \tau^-\bar{\nu}_\tau X$ decays, (ii) $b, \bar{c} \rightarrow e^-/\mu^- X$ decays in which the $e^\pm/\mu^\pm$ were not identified, and (iii) "residual background" caused by poor energy measurement. Table 2 summarizes the number of entries in Fig. 3 from each of these sources. As in all the figures in this paper, the contribution from $b \rightarrow \tau^-\bar{\nu}_\tau X$ decays in the Monte Carlo has been scaled by the ratio of the measured branching ratio (given below) to that assumed in the Monte Carlo (2.78%).

To reduce sensitivity to systematic effects (such as the fraction of hemispheres with $E_{neut} > 7$ GeV), the Monte Carlo histogram was normalized to have the same number of entries as the data, before calculating the $b \rightarrow \tau^-\bar{\nu}_\tau X$ branching ratio. The branching ratio was then obtained from a comparison of the number of hemispheres in the signal region, $E_{miss} > E_{cut}$, of the Monte Carlo and data histograms.

In Table 3, the resultant values of the $b \rightarrow \tau^-\bar{\nu}_\tau X$ branching ratio are given for three different values of E_{cut}. (These results exclude contributions from cascade decays such as $b \rightarrow D_s^- X$, $D_s^- \rightarrow \tau^-\bar{\nu}$). The systematic errors given in this table are obtained in Section 5.1. As the result obtained using $E_{cut} = 12$ GeV has the smallest total error, it will be taken as the best estimate of the branching ratio:

$$\text{B.R.}(b \rightarrow \tau^-\bar{\nu}_\tau X) = 4.08 \pm 0.76 \pm 0.62\%.$$

5.1 Systematic Effects and Corrections

This subsection examines the systematic errors on the branching ratio. The results given here were obtained using $E_{cut} = 12$ GeV and are summarized in Table 4. Using larger values of E_{cut} reduces sensitivity to the residual background, but

increases statistical errors and sensitivity to the b fragmentation function (as a smaller fraction of the semileptonic decay spectrum is being sampled).

5.1.1 Uncertainty in the Residual Background

Following the discussion of Section 4.1, the effect of uncertainties in the residual background will be estimated by:

(i) Removing the weights applied to the residual background spectrum in the region $E_{miss} > 10$ GeV. This produces an absolute change in the measured $b \to \tau^- \bar{\nu}_\tau X$ branching ratio of $0.42 \pm 0.05\%$[1].

(ii) Omitting the scale factor f_{extra} which was applied to E_{vis}, which gives an absolute change in the measured branching ratio of $0.27 \pm 0.07\%$.

In view of Section 4.1, it is likely that the poor simulation of E_{neut} will dominate uncertainties in the residual background. A check was therefore made by repeating the analysis without the cut $E_{neut} < 7$ GeV. This yields an absolute change in the measured branching ratio of $-0.57 \pm 0.31\%$.

A further check was made to see if the results were unduly sensitive to the choice of recalibration procedure in Section 4.1. Scaling the E_{vis} when recalibrating the Monte Carlo, rather than scaling the individual contributions to it ($E_{charged}$, E_{photon} and E_{neut}), yields a branching ratio of $4.00 \pm 0.74\%$, which is statistically consistent with that in Table 3.

5.1.2 Uncertainty in Neutrino Energy Spectrum

The missing energy spectrum of hemispheres containing semileptonic b decays depends primarily upon $<x_B>=<E_B>/E_{beam}$ of the primary b hadrons. This quantity has been measured to be $0.70 \pm 0.01 \pm 0.02$ [10]. Changing $<x_B>$ by ± 0.022 (by adjusting ϵ_B in the Peterson fragmentation function) produces an absolute change in the measured branching ratio of $\mp 0.14 \pm 0.08\%$.

An independent check that the simulation of the $b, \bar{c} \to e^-/\mu^- X$ missing energy spectrum is correct, was obtained by taking $b\bar{b}$ tagged hemispheres and *requiring* the presence of an $e^\pm/\mu^\pm$. The resultant E_{miss} spectrum is shown in Fig. 4. Its tail is dominated by $b, \bar{c} \to e^-/\mu^- X$ decays. Data and Monte Carlo are in good agreement.

5.1.3 Uncertainty in $b \to e^-/\mu^- X$ Branching Ratio

The $b \to e^-/\mu^- X$ branching ratio is measured to be $11.0 \pm 0.4 \pm 0.4\%$ [10]. Changing this branching ratio by $\pm 0.57\%$ produces an absolute change in the measured $b \to \tau^- \bar{\nu}_\tau X$ branching ratio of $\mp 0.13 \pm 0.02\%$.

The agreement between Monte Carlo and data in Fig. 4 provides a check that the assumed $b \to e^-/\mu^- X$ branching ratio is reasonable.

---

[1] The error given on this number is the statistical error on the change in the measured branching ratio, taking into account correlations between the two measurements. This is also the case for the similar results given elsewhere in this subsection and in Table 4.

5.1.4 $e^\pm/\mu^\pm$ Identification Efficiencies

The systematic error arising from the uncertainty in the $e^\pm/\mu^\pm$ identification efficiencies was taken as one half of the change in the branching ratio resulting from the corrections of Section 4.2. This implies an absolute uncertainty in the $b \to \tau^- \bar{\nu}_\tau X$ branching ratio of $\pm 0.07 \pm 0.02\%$ arising from $\mu^\pm$ identification and $\pm 0.03 \pm 0.02\%$ from $e^\pm$ identification.

As the simulation of the $\mu^\pm$ identification efficiency is poorest at low momenta, an independent check was made by repeating the analysis without attempting $\mu^\pm$ identification below 3 GeV. This produces an absolute change in the measured branching ratio of $0.26 \pm 0.48\%$. A similar test for $e^\pm$ changed the result by $-0.05 \pm 0.57\%$.

A final check was made by selecting $b\bar{b}$ tagged hemispheres satisfying $E_{miss} >$ 16 GeV and plotting the momentum of the highest momentum identified lepton (which frequently comes from $b, \bar{c} \to e^-/\mu^- X$). This is shown in Figs. 5a,b for the case where this lepton is an $e^\pm/\mu^\pm$ respectively. The discrepancies present between Monte Carlo and data are small.

5.1.5 $e^\pm/\mu^\pm$ from other Sources

The Monte Carlo indicates that the probability of a hemisphere being rejected because it contains $e^\pm/\mu^\pm$ from $\pi^\pm$ or $K^\pm$ decays, gamma conversions or hadron misidentification, decreases by 2% as E_{miss} rises from -30 to $+30$ GeV. If this dependence is different in the data, this will lead to a systematic error on the branching ratio.

The small dependence on E_{miss} in the Monte Carlo suggests that this is unlikely to be an important effect. The dependence arises because hemispheres with little visible energy tend to have little charged energy and thus fewer tracks which could be identified $e^\pm/\mu^\pm$.

The effect was studied using hemispheres selected with a light quark event tag ($\alpha^{event} > 0.5$) to reduce interference from semileptonic decays. The probability of hemispheres containing $e^\pm/\mu^\pm$ was plotted versus $E_{charged}$, and was seen to rise from zero to 51%, as $E_{charged}$ changed from zero to E_{beam}. (Looking at $E_{charged}$ has the twin advantage that the probability shows a much larger dependence on it than on E_{miss}, and that residual hemispheres containing semileptonic decays will not cluster in any one part of the spectrum). The ratio of this plot in data to Monte Carlo could be well parameterized by $\kappa(1 + \lambda E_{charged})$, where $\kappa = 1.02 \pm 0.02$ and $\lambda = -0.0008 \pm 0.0007$.

Weighting Monte Carlo hemispheres by a factor $(1 \pm 0.0015 E_{charged})$ produces an absolute change in the measured branching ratio of $\pm 0.15 \pm 0.03\%$.

5.1.6 $b\bar{b}$ Selection Efficiencies

Varying the performance of the $b\bar{b}$ tag in the Monte Carlo in accordance with the errors given in Section 4.3 yields an absolute change in the measured branching ratio of $\pm 0.05 \pm 0.01\%$.

11

The correction factors of Section 4.3 are appropriate for an 'average' $b\bar{b}$ event. That they might not be correct for $b\bar{b}$ events containing semileptonic decays is suggested by the fact that the tag gives a slightly worse performance on such events. (The Monte Carlo predicts that the $b\bar{b}$ tagging efficiency is 1% lower than average for $b\bar{b}$ events containing semileptonic decays). This was investigated by correcting the resolution function, $\rho(D)$, on the distance of closest approach of tracks to the primary vertex (Section 3), to make it the same in the Monte Carlo as in the data. The $b\bar{b}$ tagging efficiencies predicted by the Monte Carlo with and without this correction were in the ratio 0.849, thus accounting for a large proportion of the discrepancy seen in Section 4.3. For $b\bar{b}$ events containing semileptonic decays, this ratio took the value 0.846, showing that the correction factors of Section 4.3 are indeed correct for such events. For $b\bar{b}$ events which not only contained a semileptonic decay, but also contributed to the signal region of Fig. 3, this same ratio took a value 0.83 ± 0.04. Assuming that the difference between this number and 0.849 is real, implies an absolute systematic error on the measured branching ratio of $\pm0.16 \pm 0.28\%$.

As a check, the $b \to \tau^-\bar{\nu}_\tau X$ analysis was repeated but with the $b\bar{b}$ tag being applied only to the hemisphere opposite to that in which E_{miss} was measured, rather than to the entire event. This ensured that the tagging efficiency was uncorrelated with the characteristics of the hemisphere being studied. It yielded a branching ratio of $2.88 \pm 0.91\%$ (differing by $-1.20 \pm 0.65\%$ from that in Table 3).

5.1.7 Other Sources of $\tau^\pm$

$D_s^- \to \tau^-\bar{\nu}$ decays are expected to be the only other significant source of $\tau^\pm$. This process is predicted to have a branching ratio of $3^{+4}_{-2}\%$ [11], which according to the Monte Carlo, implies that in the region $E_{miss} > 12$ GeV of Fig. 3, there are six entries corresponding to $D_s^- \to \tau^-\bar{\nu}$ decays. Changing the branching ratio of $D_s^- \to \tau^-\bar{\nu}$ by $\pm3\%$ alters the measured $b \to \tau^-\bar{\nu}_\tau X$ branching ratio by $\mp0.21 \pm 0.10\%$.

5.1.8 Detector Problems

The number of entries in the positive tail of the E_{miss} spectrum in Fig. 1b is sensitive to the detector resolution and detector inefficiencies. The data were checked for unexpected detector failures by studying the number of such entries as a function of time and as a function of the direction of the missing energy vector. No fluctuations inconsistent with Poisson statistics were seen in these plots. Any systematics arising from this source are in any case already included in those of Section 5.1.1.

6 Conclusions

The $b \to \tau^-\bar{\nu}_\tau X$ branching ratio has been measured to be $4.08 \pm 0.76 \pm 0.62\%$.

This result is compatible with the standard model prediction of $2.83 \pm 0.31\%$, and rules out the more exotic predictions of [2].

Acknowledgements

References

[1] P. Heiliger, L.M. Sehgal, Phys. Lett. **B229** (1989) 409

[2] B. Grzadkowski, W.-S. Hou, Phys. Lett. **B283** (1992) 427

[3] D. Decamp *et al.*, ALEPH Collab., Nucl. Instr. and Meth. **B294** (1990) 121

   G. Batignani *et al.*, "Recent Results and Running Experience of the new ALEPH Vertex Detector",1991 IEEE Nuclear Science Symposium, Santa Fe, U.S.A.

[4] D. Decamp *et al.*, ALEPH Collab., Phys. Lett **B231** (1989) 519, Section 3.1

[5] T. Sjörstrand and M. Bengtsson, Comp. Phys. Com. **43** (1987) 367

   JETSET 7.2 User's Manual

[6] C. Peterson *et al.*, Phys. Rev. **D27** (1983) 105

[7] D. Decamp *et al.*, ALEPH Collab., Phys. Lett. **B246** (1990) 306, Section 2.1

[8] D. Decamp *et al.*, ALEPH Collab., Phys. Lett. **B244** (1990) 551, Sections 4 and 5

[9] W. Bartel *et al.*, JADE Collab., Z. Phys. **C33** (1986) 23. The parameter y_{cut} in the algorithm was set to 0.02 .

[10] "Heavy Flavour Physics with Leptons", ALEPH Collab., XXVIth International Conference on High Energy Physics, Dallas (1992)

[11] G. Martinelli *et al.*, Nucl. Phys. **B376** (1992) 172

Table 1: Recalibration parameters needed for Monte Carlo.

	Value
$f_{charged}$	0.999 ± 0.002
f_{photon}	0.998 ± 0.003
f_{neut}	0.900 ± 0.020

Table 2: Number of entries in Fig. 3. The Monte Carlo numbers are scaled so as correspond to a $b \to \tau^- \bar{\nu}_\tau X$ branching ratio of 4.08%. They have also been normalised to have the same total number of entries as the data.

Bin (GeV)	Data	Monte Carlo			
		$b \to \tau^- \bar{\nu}_\tau X$	$b, \bar{c} \to e^-/\mu^- X$	Residual Background	Total
$-30 < E_{miss} < 8$	6840	107	288	6456	6851
$8 < E_{miss} < 12$	407	63	71	263	397
$12 < E_{miss} < 16$	146	53	32	56	141
$16 < E_{miss} < 20$	54	33	20	12	65
$20 < E_{miss} < 30$	55	30	20	0	50

Table 3: Results for the $b \to \tau^- \bar{\nu}_\tau X$ branching ratio.

E_{cut} (GeV)	$b \to \tau^- \bar{\nu}_\tau X$ Branching Ratio
12	$4.08 \pm 0.76 \pm 0.62$ %
16	$3.76 \pm 0.91 \pm 0.46$ %
20	$4.91 \pm 1.44 \pm 0.68$ %

14

Table 4: Systematic errors obtained when $E_{cut} = 12$ GeV

Systematic Effect	Absolute Change in $b \to \tau^- \bar{\nu}_\tau X$ Branching Ratio
Uncertainty in residual background for $E_{miss} > 10$ GeV	$\pm\ 0.42 \pm 0.05\%$
Uncertainty in residual background: f_{extra}	$\pm\ 0.27 \pm 0.07\%$
± 0.022 change in $< x_B >$	$\mp\ 0.14 \pm 0.08\%$
$\pm 0.57\%$ change in $b \to e^-/\mu^- X$ branching ratio	$\mp 0.13 \pm 0.02\%$
Uncertainty in $\mu^\pm$ identification efficiency	$\pm\ 0.07 \pm 0.02\%$
Uncertainty in $e^\pm$ identification efficiency	$\pm\ 0.03 \pm 0.02\%$
Uncertainty in $e^\pm/\mu^\pm$ from other sources	$\pm\ 0.15 \pm 0.03\%$
Uncertainty in $b\bar{b}$ tag efficiency	$\pm 0.05 \pm 0.01\%$
Same again for events with semileptonic decay	$\pm 0.16 \pm 0.28\%$
$\pm 3\%$ change in $D_s^- \to \tau^- \bar{\nu}$ branching ratio	$\mp 0.21 \pm 0.10\%$
Total Systematic Error	$\pm 0.62\%$

Figure Captions

Fig. 1: E_{miss} spectrum (a) prior to and (b) after the corrections of Section 4.1 (including the $E_{neut} < 7$ GeV cut), for hemispheres selected using the light quark event tag and $e^{\pm}/\mu^{\pm}$ rejection cut.

Figs. 2a,b: Comparison of $e^{\pm}/\mu^{\pm}$ identification efficiencies in Monte Carlo with those in the data.

Fig. 3: E_{miss} spectrum after application of all the cuts of Section 3.

Fig. 4: E_{miss} spectrum of $b\bar{b}$ tagged hemispheres in which the presence of $e^{\pm}/\mu^{\pm}$ is *required*.

Figs. 5a,b: Momentum spectrum of highest momentum lepton if it is an $e^{\pm}/\mu^{\pm}$ respectively. Only $b\bar{b}$ tagged hemispheres with $E_{miss} > 16$ GeV have been used.
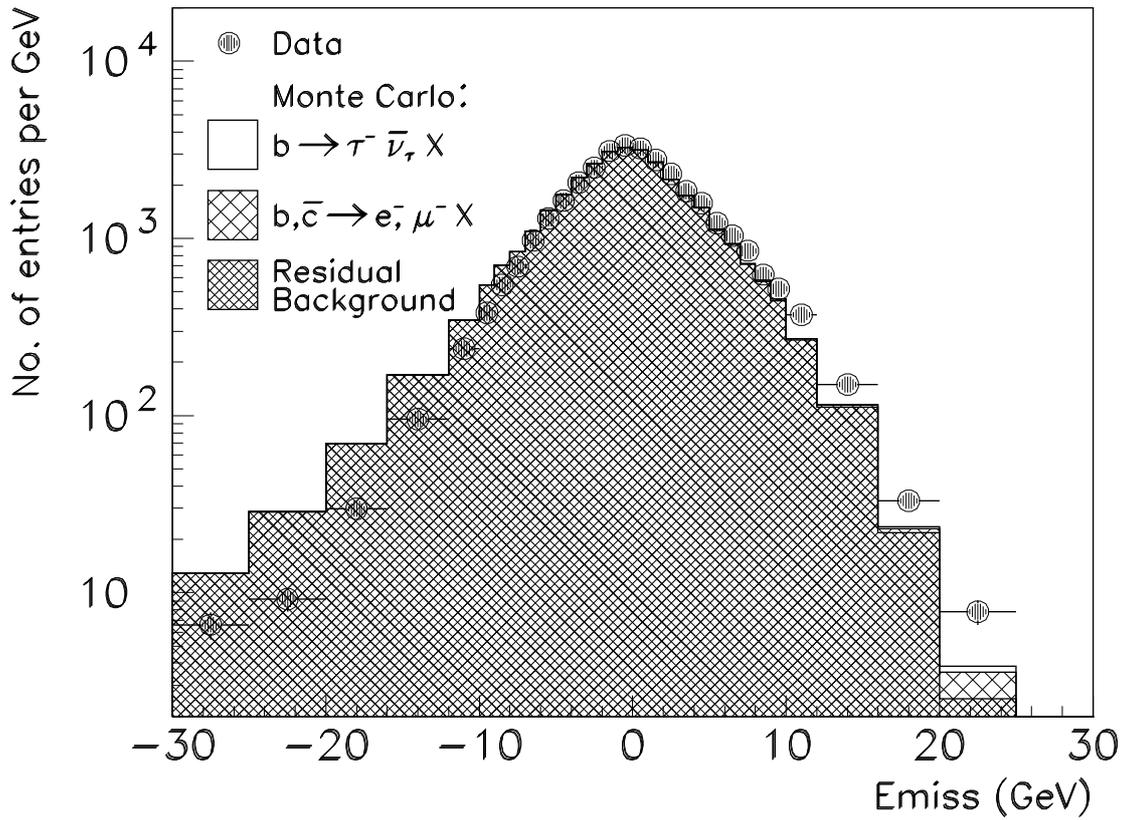
Fig. 1a : Emiss before recalibration
Using light quark tag and $e^{\pm}, \mu^{\pm}$ rejection
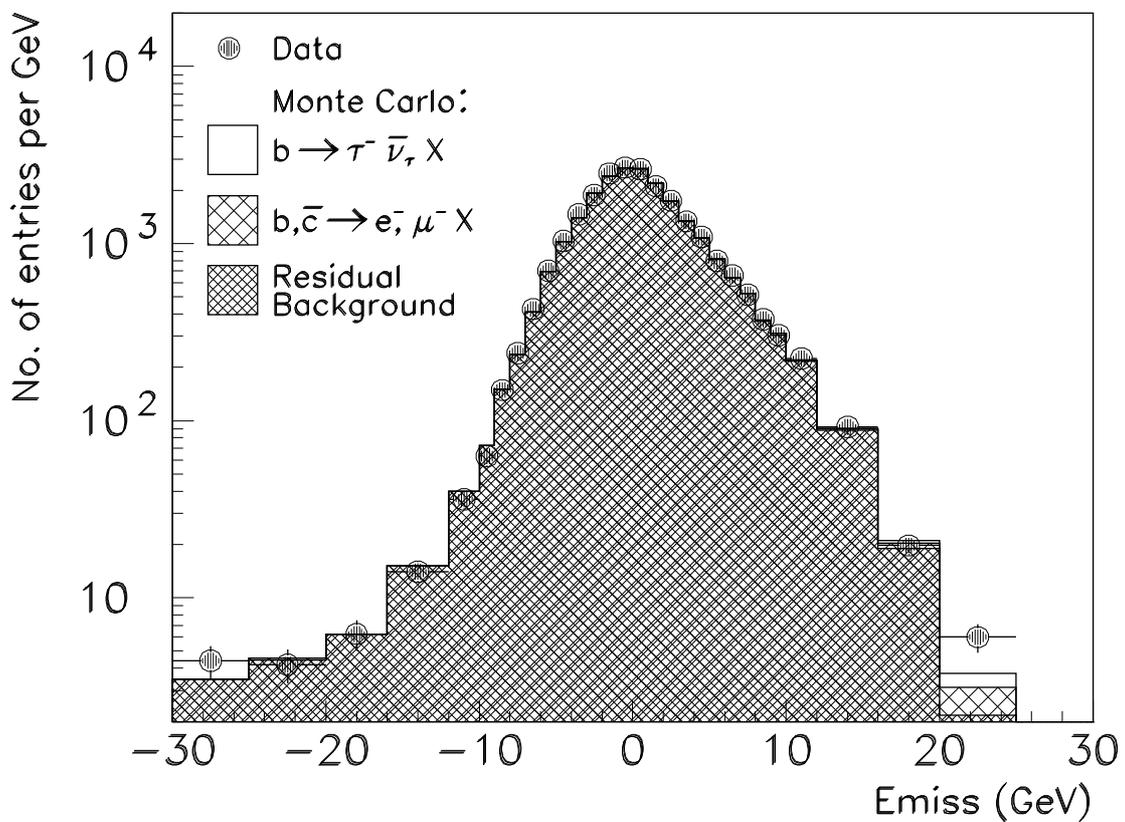
Fig. 1b : Emiss after recalibration
Using light quark tag and $e^{\pm}, \mu^{\pm}$ rejection
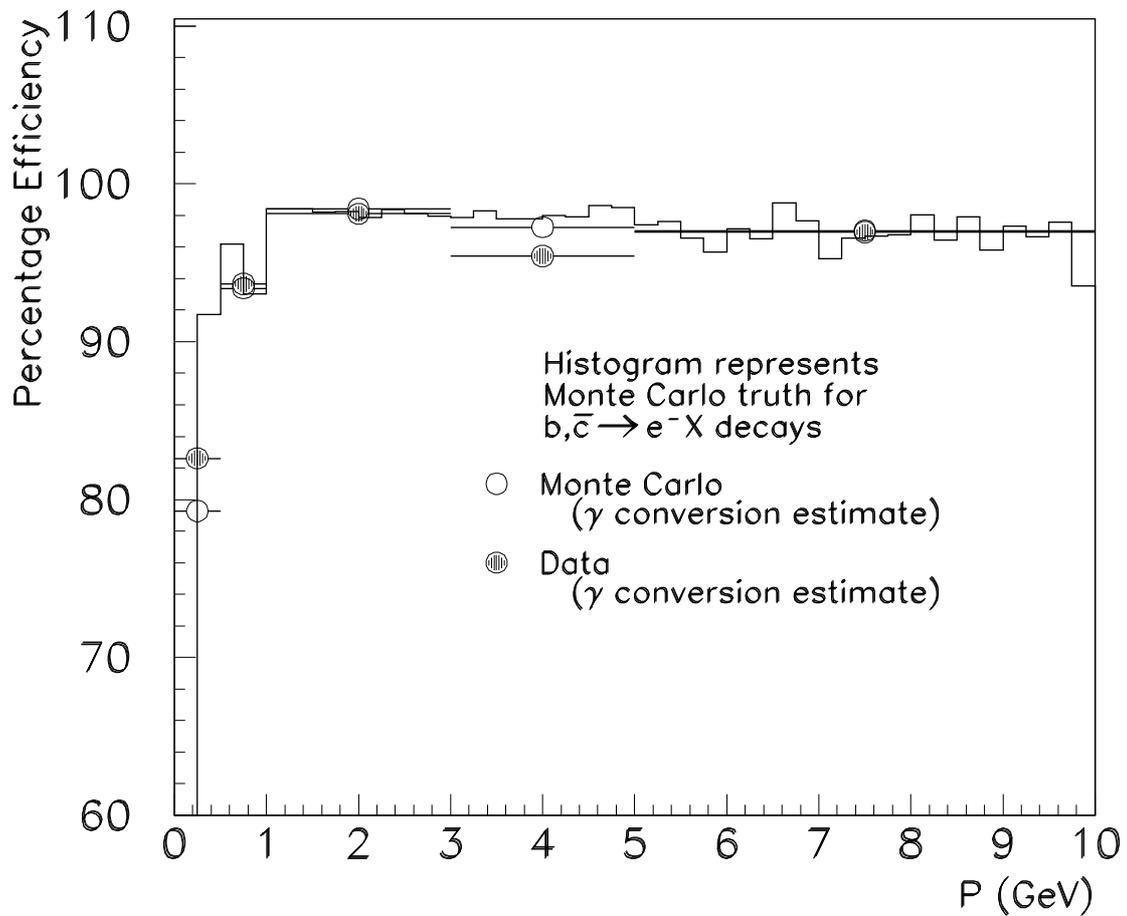and Eneut < 7 GeV cut
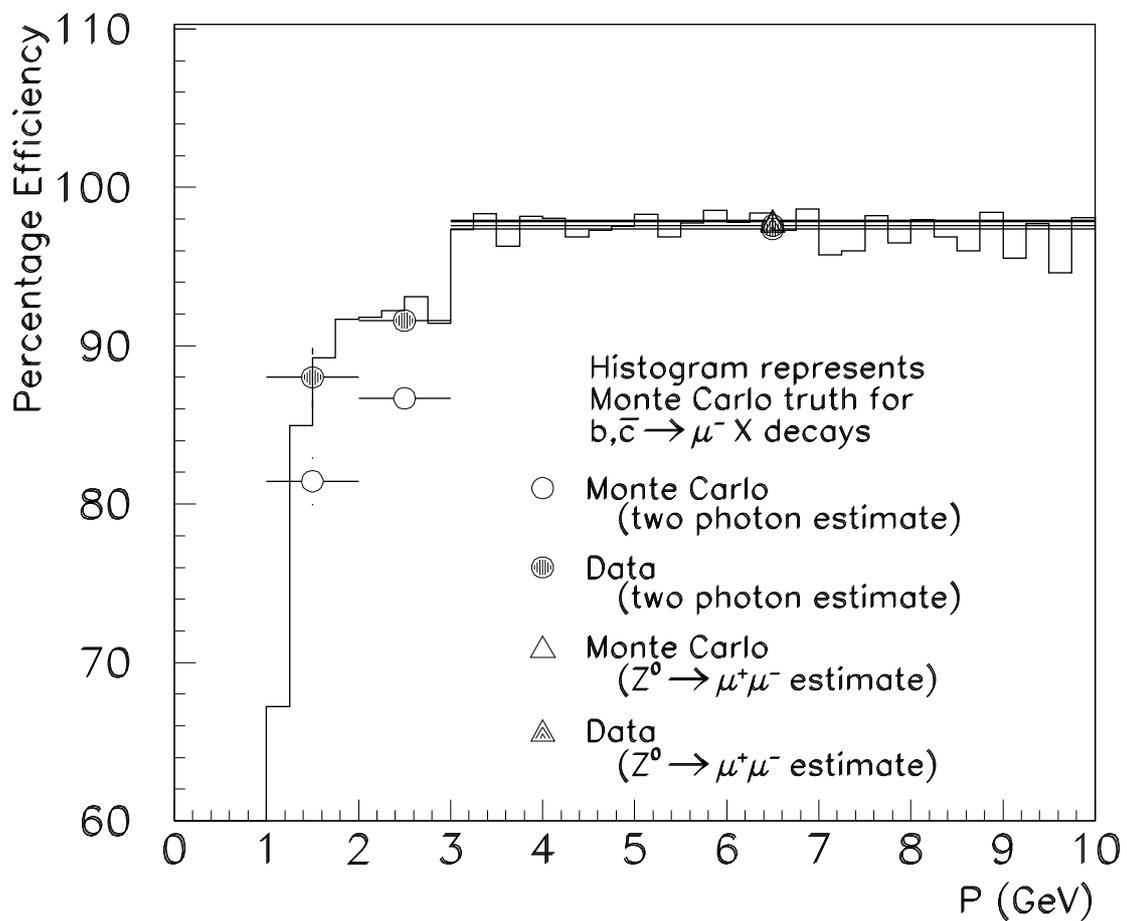
Fig. 2a : $e^{\pm}$ identification efficiency
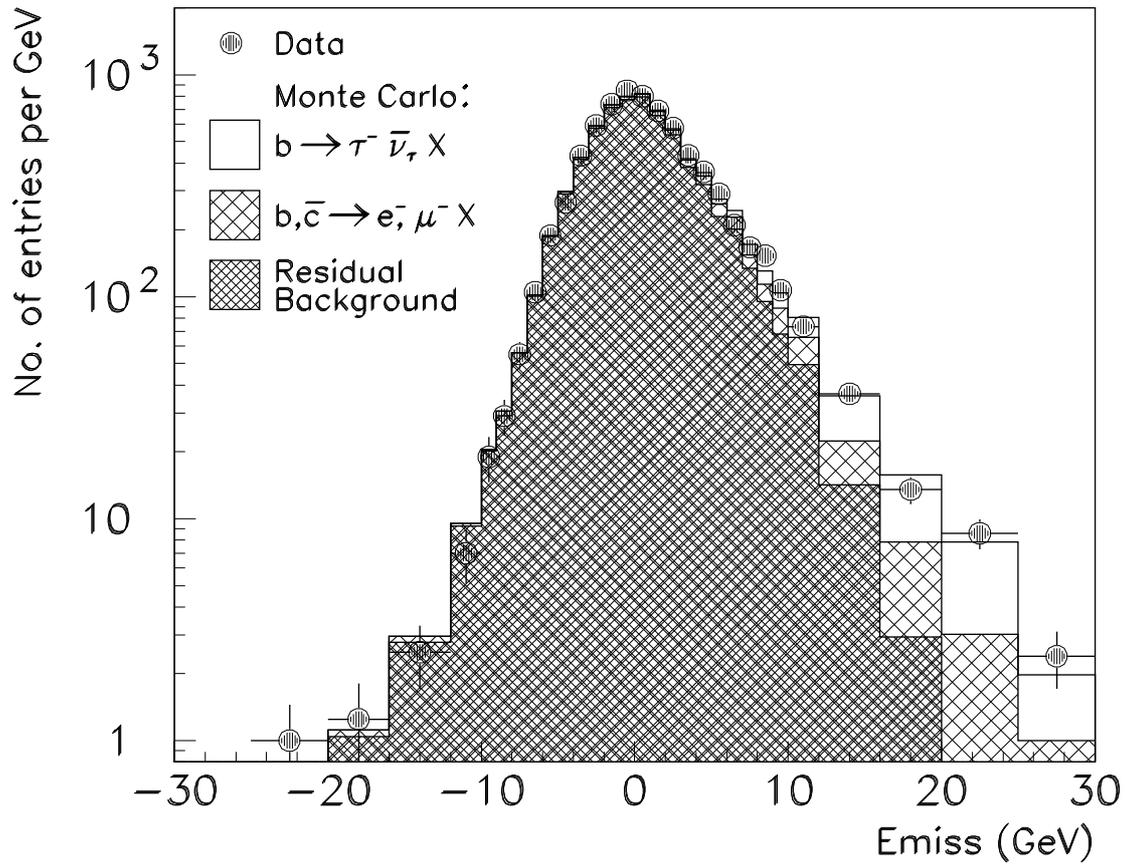

Fig. 2b : $\mu^{\pm}$ identification efficiency

Fig. 3 : Emiss after all the cuts of Section 3

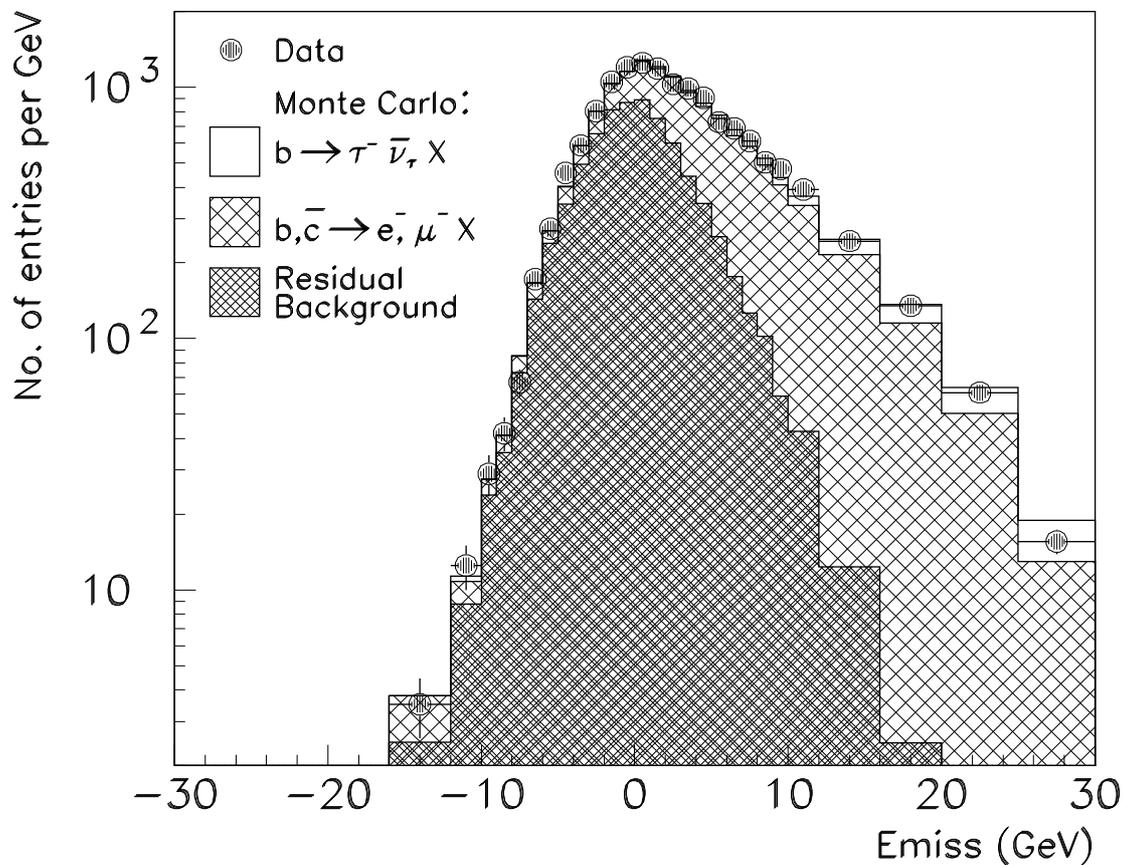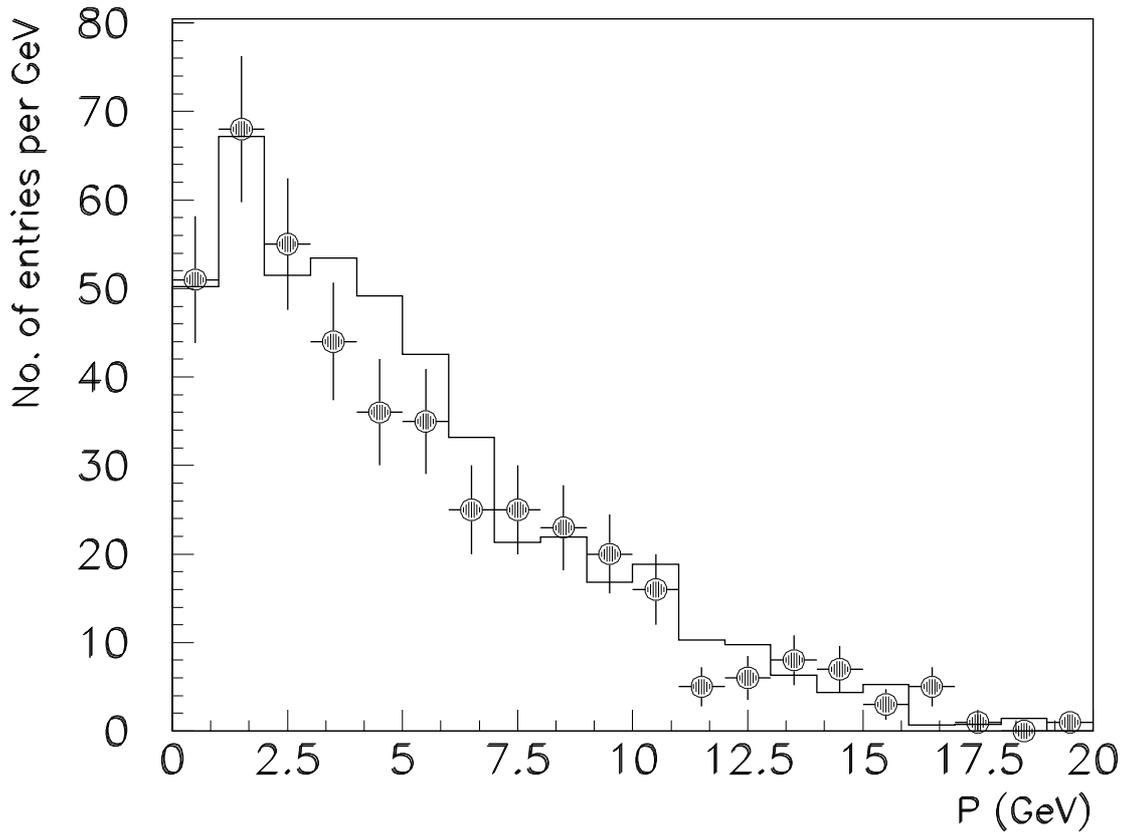Fig. 4 : Emiss using b̄b tag
and requiring presence of e$^\pm$, $\mu^\pm$

Fig 5a : P of highest momentum lepton if e$^{\pm}$
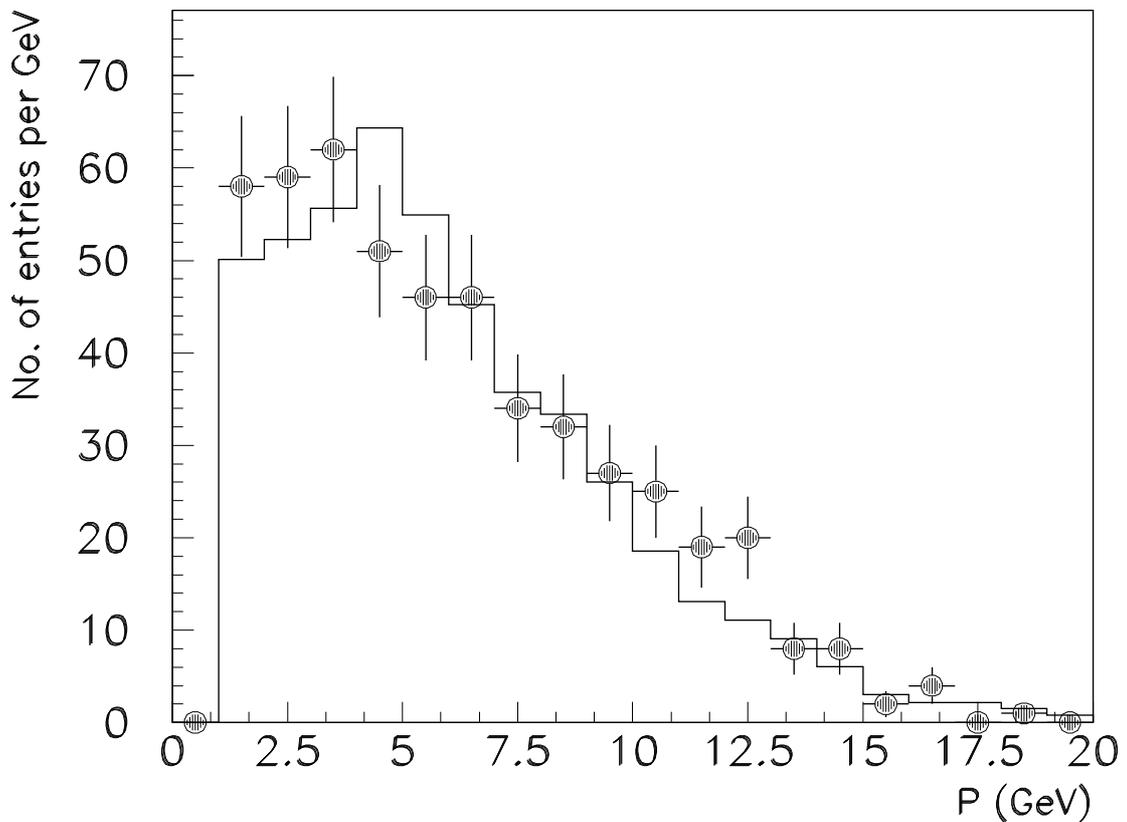b$\bar{\text{b}}$ tagged hemisheres with Emiss > 16 GeV

Fig 5b : P of highest momentum lepton if $\mu^{\pm}$
b$\bar{\text{b}}$ tagged hemispheres with Emiss > 16 GeV